

Evaluation of global climate model on performances of precipitation simulation and prediction in the Huaihe River basin

Yenan Wu¹ · Ping-an Zhong^{1,2}  · Bin Xu¹ · Feilin Zhu¹ · Jisi Fu¹

Received: 10 October 2016 / Accepted: 22 May 2017 / Published online: 7 June 2017
© Springer-Verlag Wien 2017

Abstract Using climate models with high performance to predict the future climate changes can increase the reliability of results. In this paper, six kinds of global climate models that selected from the Coupled Model Intercomparison Project Phase 5 (CMIP5) under Representative Concentration Path (RCP) 4.5 scenarios were compared to the measured data during baseline period (1960–2000) and evaluate the simulation performance on precipitation. Since the results of single climate models are often biased and highly uncertain, we examine the back propagation (BP) neural network and arithmetic mean method in assembling the precipitation of multi models. The delta method was used to calibrate the result of single model and multimodel ensembles by arithmetic mean method (MME-AM) during the validation period (2001–2010) and the predicting period (2011–2100). We then use the single models and multimodel ensembles to predict the future precipitation process and spatial distribution. The result shows that BNU-ESM model has the highest simulation effect among all the single models. The multimodel assembled by BP neural network (MME-BP) has a good simulation performance on the annual average precipitation process and the deterministic coefficient during the validation period is 0.814. The simulation capability on spatial distribution of precipitation is: calibrated MME-AM > MME-BP > calibrated BNU-ESM. The future precipitation predicted by all models

tends to increase as the time period increases. The order of average increase amplitude of each season is: winter > spring > summer > autumn. These findings can provide useful information for decision makers to make climate-related disaster mitigation plans.

1 Introduction

Precipitation plays a key role in climate system and precipitation variability in the context of climate change induces substantial impacts on both nature environments and human society (Chen and Frauenfeld 2014), underscoring the need to better evaluate the future climate trends to response climate change and ensure water security. Projections of future climate change using climate model coupled with atmosphere-ocean circulation system also suggest that climate in the future will more severe due to the increased greenhouse gas concentrations (Hirabayashi et al. 2013). However, because of model structural errors, parameterization uncertainty, and different region scales, the output of climate model tend to exhibit substantial bias in the spatial-temporal distribution of regional precipitation (Steinschneider and Lall 2015). Therefore, it is very important to select an effective model for regional application such that it can both simulate the climate reasonably in the past and test the reliability of future climate trend prediction.

At present, the advanced climate prediction data of atmosphere-ocean general circulation models (AOGCMs) is provided by the World Climate Research Programme (WCRP), which participates in the fifth phase of the Coupled Model Intercomparison Project (CMIP5) (Stocker et al. 2013). When using a single global climate model to assess the trend of future climate in a particular watershed, the results are often biased and highly uncertain, thus they

✉ Ping-an Zhong
pazhong@hhu.edu.cn

¹ College of Hydrology and Water Resources, Hohai University, No.1 Xikang Road, Nanjing 210098, China

² National Engineering Research Center of Water Resources Efficient Utilization and Engineering Safety, Hohai University, No.1, Xikang Road, Nanjing 210098, China

cannot provide reliable information to decision makers (Sarwar et al. 2012). The multimodel ensemble (MME) technique has been an effective ways for improving weather and climate forecast to reduce uncertainty (Feng et al. 2011; Sun et al. 2015). Lu et al. (2014) used MMEs including 21 global climate models in CMIP5 coupled with VIC model to predict the spatial and temporal variation of snow depth in the upper reaches of the Yangtze River in the next 30 years. Lim et al. (2015) proposed a MME method based on independent component analysis and regression analysis, and they then predicted the future summer rainfall over global and regional scales. Wang et al. (2014) predicted the future extreme climate trends under different emission scenarios by MME projections via Bayesian model average method.

Additionally, plenty of studies have been carried out on comparing different MME methods. Du et al. (2010) used a weighting ensemble method of pattern correlation coefficients in moving windows, and they found that the result is better than the result of multimodel assembled by the arithmetic mean method and the traditional correlation coefficient. Min et al. (2014) compared the difference between the multiple regression method, arithmetic mean method, and stepwise projection method when assembling different single models. The results show that the stepwise projection method is the best and the arithmetic average method is better than the multiple regression method. Ke et al. (2009) analyzed the difference between multiple linear regression model and arithmetic mean method when assembling multimodels, and found that the MMEs calculated by the multiple linear regression model is not suitable for the high latitude region. Besides, a lot of studies (Kharin and Zwiers 2002; Peng et al. 2002) show that the result is unsatisfactory when using the weight optimization or complex models for assembling the multimodel data, and it is even worse than the simple arithmetic mean method.

Huaihe River basin is one of the most important energy bases and food-production bases which is attacked by flood disaster frequently in China (Wu et al. 2015). In recent years, a lot of researches have been devoted to predict the climate trend over the Huaihe River basin. Gao et al. (2012) used the measured data to evaluate the trend of average temperature, extreme temperature, and precipitation during historical periods and applied the ECHAM5 model to predict the trend of precipitation and temperature in the future. Wu and Yan (2013) predicted the temperature and precipitation changes under the A2, A1B, and B1 SRES scenarios in the next 30 years by using eight kinds of climate model data of IPCC AR4. Li et al. (2012a) predicted the trend of precipitation and temperature during three future time periods (2020s, 2050s, and 2080s) by using the CSIRO and HadCM3 climate model and used the predicted temperature result as the input of an evaporation function model to simulate the evaporation process in the future.

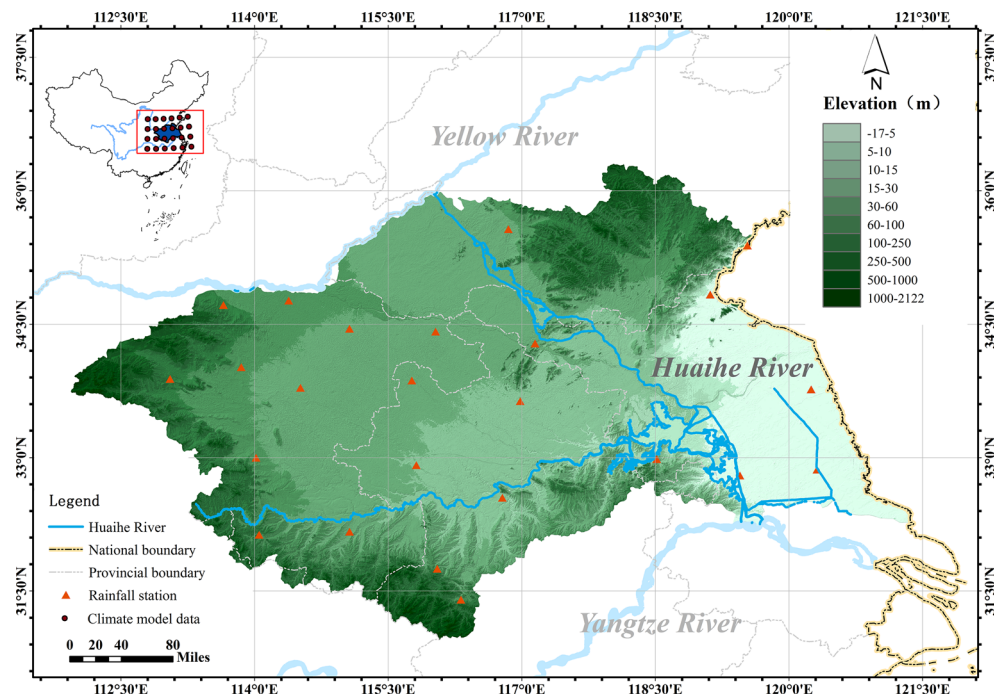
Recently, the back propagation (BP) neural network has been widely used in the medium long-term forecasting of the hydrological terms (Luo et al. 2016; Shoaib et al. 2016) as it has the advantages of good fault tolerance, self-adaptation, and parallel data processing ability. However, previous studies seldom use the BP neural network to assemble the multi climate models. Therefore, we selected the Huaihe River basin as the study area and divided the climate data which spans from 1960 to 2010 into three periods: baselines period (1960–2000), validation period (2001–2010), and prediction period (2011–2100). The main objectives of this paper are to (1) evaluate the simulation performance of six global climate models provided by IPCC AR5 under RCP 4.5 scenario; (2) assemble the global climate data by using arithmetic mean method (MME-AM) and BP neural network (MME-BP); (3) use the Delta method to calibrate the bias of single climate models and MME-AM and rebuild the future precipitation series; (4) predict the long-term linear trend, interannual distribution, and spatial distribution trend of precipitation during the prediction period over the Huaihe River basin using the calibrated single climate model with high simulation performance, calibrated MME-AM, and MME-BP.

The balance of this paper is organized as follows: in the next section, we describe the study area and the data for this study. Section 3 mainly describes the Methodology of BP neural network. The evaluation and calibration of global climate models and MME-AM are presents in Section 4. In Section 5, simulation results by BP neural network are presented, followed by Section 6 that predicted the future change of precipitation. In the last section (Section 7), we summarize the main findings.

2 Study area and data

The historical monthly precipitation data measured at 29 rainfall stations in or around the Huaihe River basin are gathered over a period from 1960 to 2010. The position of rainfall stations is shown in Fig. 1. The global climate data involved with six AOGCMs under Representative Concentration Pathways (RCP) 4.5 are provided by IPCC AR5, including BCC-CSM-1.1, BNU-ESM, MIROC-ESM, CNRM-CM5, MPI-ESM-LR, and MRI-CGCM3. The global climate model (GCM) output of the precipitation is calculated from 1960 to 2100. The detail information of each climate model is shown in Table 1. We set the baseline period starting from 1960 to 2010 and establish the validation period starting from 2001 to 2010 as well as defining the prediction period which starts from 2011 to 2100.

Fig. 1 The location of study area, rainfall station, and global climate model



3 Methodology

3.1 Delta method

As the spatial resolution of GCM output is so coarse that it increases the difficulty in predicting the regional climate precisely, the delta method is commonly applied to correct the bias of GCM scenario prediction results (Hay et al. 2000; Liu et al. 2012).

The delta method uses the difference between the simulation results of GCM models and the measured data during the baseline period to rebuild the future climate data series. Specifically, for precipitation data, we calculate the precipitation change rate of each grid between average simulation result and average measure data during the baseline period. We then multiply the GCM perdition output with the change rate to rebuild the future

perdition precipitation series. The equation for future precipitation scenarios on each grid is shown below:

$$P_f = P_0 \cdot \frac{P_{Gf}}{P_{G0}} \tag{1}$$

The term P_f is the rebuilt future precipitation data; the term P_{Gf} is the GCM output of future precipitation data; the term P_{G0} is the GCM output of multiyear average precipitation during the baseline period, and the term P_0 is the observation of multiyear average annual precipitation during the baseline period.

3.2 BP neural network

BP neural network is a multilayer feed forward artificial neural network with error back propagation algorithm, which has

Table 1 Lists the multiyear average precipitation value between climate model and measured data

Number	Model name	Simulation value (mm)	RE (%)	CC	DC	SD (mm)	RMSE (mm)
A	BCC-CSM-1.1	1082.3	20.7	0.344	0.348	133.0	227.4
B	BNU-ESM	1045.3	16.6	0.766	0.610	141.2	197.1
C	MIROC-ESM	960.6	7.1	0.603	-0.458	113.6	193.4
D	CNRM-CM5	868.7	-3.1	0.665	0.007	136.3	194.0
E	MPI-ESM-LR	946.6	5.6	-0.133	-1.349	131.2	209.4
F	MRI-CGCM3	527.4	-41.2	0.610	0.336	71.7	167.7
G	MME-AM	938.5	4.7	0.799	0.281	57.1	166.2

presented a particularly popular artificial neural network method within past 20 years. BP neural network is composed of an input layer, a hidden layer, and an output layer. In this paper, we establish a BP neural network with three layers. The number of nodes in the input layer is the number of global climate models. The input value is the predicted precipitation value of each climate model. The output layer has one node and the expected output value is the fitting network of MME. Each node of the input layer uses the linear activation function, and the nodes of the hidden layer as well as that of the output layer use sigmoid activation function.

Firstly, we normalize the input data between α and β using the following equation.

$$a_i(t) = \alpha + (\beta - \alpha) \cdot \frac{x_i(t) - X_{\min}}{X_{\max} - X_{\min}} \quad (2)$$

where the term $x_i(t)$ is the precipitation value of i th climate model at time t ; the term X_{\max} and X_{\min} are the maximum and minimum value of input series, respectively; the term α and β are the parameters of data normalization, which satisfies $\alpha + \beta = 1$; and the term $a_i(t)$ is the normalized precipitation value of i th climate model at time t .

We then normalize the expected output value $T(t)$ between α and β as what is done to the input data:

$$b(t) = \alpha + (\beta - \alpha) \cdot \frac{T(t) - T_{\min}}{T_{\max} - T_{\min}} \quad (3)$$

where T_{\max} and T_{\min} are the maximum and minimum value of expected output series, respectively; the term $b(t)$ is the normalized expected value at time t .

The output of this neural network is shown in Eq. (4):

$$y(t) = f \left(\sum_{j=1}^m w_j f \left(\sum_{i=1}^n v_{ij} a_i(t) + \theta_j \right) + \theta_0 \right) \quad (4)$$

where $y(t)$ is the normalized MME value of precipitation at time t ; $f(\cdot)$ is the transferring function, the Sigmoid function; the term w_j is the weight coefficient for connecting the hidden layer and the output layer; the term v_{ij} is the weight coefficient for connecting the hidden layer and the input layer; n is the number of climate model; m is the dimension of the hidden layer; and the term θ_j , θ_0 are thresholds of hidden layer and output layer, respectively.

When the model training is completed and parameters are fixed, we predict the future precipitation by MME-BP. At this time, the model output is normalized to the range [0, 1], which needs to be converted to its actual value using Eq. (5).

$$\hat{y}(t) = T_{\min} + (T_{\max} - T_{\min})(y(t) - \alpha) / (\beta - \alpha) \quad (5)$$

where $\hat{y}(t)$ is precipitation value of MME at time t .

3.3 Inverse distance weight method

In spatial interpolation process, inverse distance weight method is one of the most widely used interpolation methods (Samanta et al. 2012; Yang et al. 2015). The general idea of this method is based on the hypothesis that the variant value of interest of an interpolation point is the weight average of the sampled point, which the interpolation point are closer to the sampled point has a larger weights (Croke et al. 2011; Waseem et al. 2016). The equations for the IDW method are as follows:

$$P(x, y) = \frac{\sum_{j=1}^n \omega_j P(x_j, y_j)}{\sum_{j=1}^n \omega_j} \quad (6)$$

$$\omega_j = \frac{1}{d^c} = \frac{1}{\left(\sqrt{(x_j - x)^2 + (y_j - y)^2} \right)^c} \quad (7)$$

where $P(x, y)$ is the variable of interest at the unknown site with the location (x, y) ; where $P(x_j, y_j)$ is the variable of interest at the known site with the location (x_j, y_j) ; n is the number of known sites; d is the distance between the site (x, y) and site (x_j, y_j) ; c is the power parameter; ω_j is the interpolation weight assigned by the j th site.

4 Global climate model evaluation

In order to assess the precipitation simulation performance of climate models over the Huaihe River basin, we calculate the monthly precipitation of each climate model and discuss the difference between the output of climate model and measured data in temporal and spatial scales. Five indices are selected for evaluating the performance of climate model, the relative error (RE), the deterministic coefficient (DC), the standard deviation (SD), the correlation coefficient (CC), and the root mean squared error (RMSE). In specific, DC reflects the fitting degree of precipitation process while the DC value closer to 1 reflects a better fitting performance. SD shows the simulation ability of climate model on center amplitude. CC reflects the degree of correlation between the model and the observation, the absolute value of CC closer to 1 means the higher correlation level. RMSE denotes deviation between simulated value and observed value while the smaller of RMSE value indicates the smaller deviation. The indices of SD, CC, and RMSE are expressed as the form of Taylor diagram (Li et al. 2012b; Sun et al. 2015) which has the advantage of comparing multiple model results simultaneously to represent the difference between the simulation result and measured data (Singh et al. 2015; Tiwari et al. 2016). Select model B as an example, where a_n and b_n are the data series of

measured data and simulated data of model B, respectively. Then the formulas for calculating the indices are as follows.

The standard deviation of the measured data A is:

$$\sigma_a = \left[\frac{1}{N} \sum_{n=1}^N (a_n - \bar{a})^2 \right]^{1/2} \tag{8}$$

The standard deviation of the model B is:

$$\sigma_b = \left[\frac{1}{N} \sum_{n=1}^N (b_n - \bar{b})^2 \right]^{1/2} \tag{9}$$

The correlation coefficient between a_n and b_n is:

$$R = \frac{\frac{1}{N} \sum_{n=1}^N (b_n - \bar{b})(a_n - \bar{a})}{\sigma_a \sigma_b} \tag{10}$$

where \bar{a} and \bar{b} are the mean value of the measured data and the simulated data.

The centralized RMSE is:

$$E = \left\{ \frac{1}{N} \sum_{n=1}^N \left[(b_n - \bar{b}) - (a_n - \bar{a}) \right]^2 \right\}^{1/2} \tag{11}$$

The correlation coefficient, standard deviation, and centralized RMSE are in accordance with the equation below:

$$E^2 = \sigma_a^2 + \sigma_b^2 - 2\sigma_a\sigma_bR \tag{12}$$

The mean annual precipitation of the Huaihe River Basin during the period (1960–2000) is 896.6 mm. As can be seen from Table 1, the results of simulation value of the CNRM-CM5 model and MRI-CGCM3 model are smaller than the mean annual precipitation, and the results of simulation value of other models are larger than the mean annual precipitation. The simulation performances of different models are distinctive. The result of MRI-CGCM3 mode has the largest relative error which is about -41.2%. The BNU-ESM model has the highest deterministic coefficient which is about 0.610 while the MPI-ESM-LR model has the lowest deterministic coefficient which is about -1.349. The simulation effect of MME-AM on the multiyear average precipitation is relatively high, and the relative error is 4.7%, but the deterministic coefficient of the precipitation process is relatively low which is about 0.281.

According to Eq. (12), we can draw the Taylor diagram as shown in Fig. 2. The position of each model represented by letter appearing on the plot quantifies how closely that simulated precipitation of each model matches with observations. The point, REF, on the x-axis is identified as observed value. Consider model B as an example, its correlation with observation is about 0.77. The centralized root mean square between the model and the observation is proportional to the

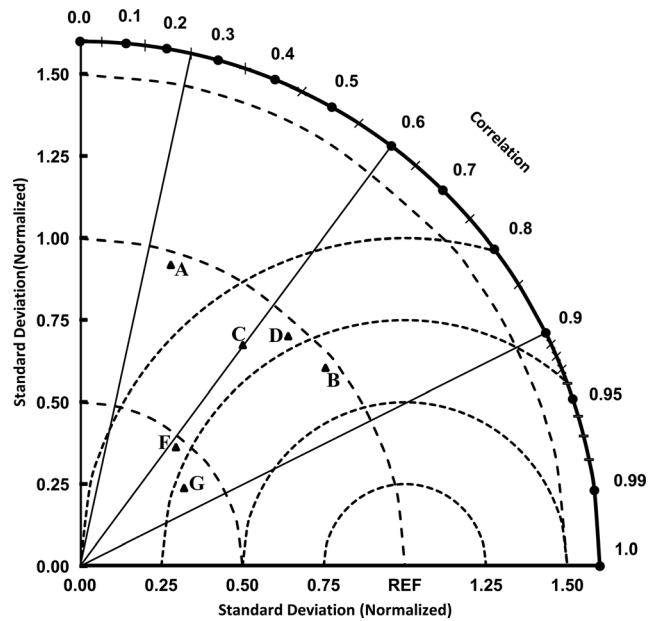


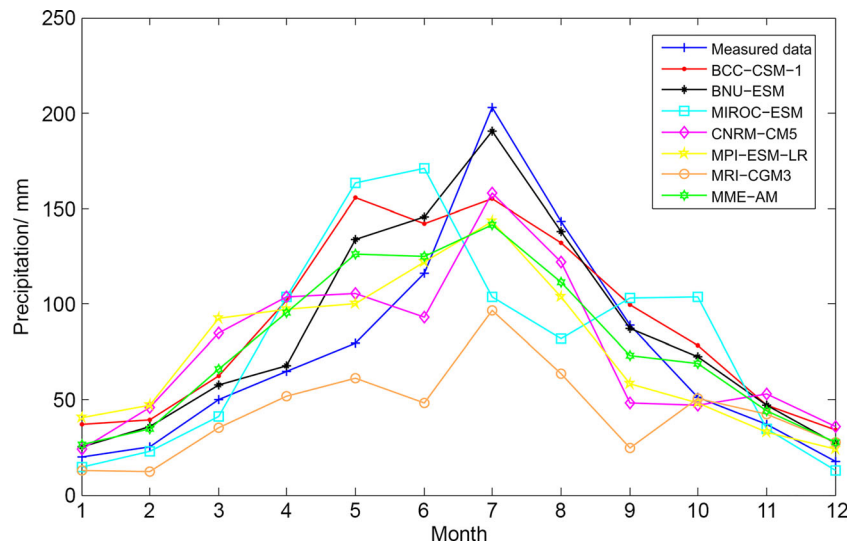
Fig. 2 The Taylor Diagram of each model during the baseline period. The correlation coefficient of model E is a negative value, thus it is not shown in the figure

distance from the model B to the REF which is about. The normalized standard deviation of model B is the radial distance from the origin which is about, while the normalized standard deviation of the observed is 1. The model with high simulation performance is near the point REF on the x-axis which has relatively high correlation low RMS errors with observed data. The position of model is closer to the dash line of 1 (radius of 1) that means has a closer normalized standard deviation to the observation. As can be seen in Fig. 2, the rank of precipitation simulation ability of each model is as follows: BNU-ESM > MME-AM > CNRM-CM5 > MRI-CGCM3 > MIROC-ESM > BCC-CSM-1.1 > MPI-ESM-LR.

4.1 Simulation of annual distribution

The multiyear average monthly precipitation simulated by each single model is compared with measured data during the baseline period as shown in Fig. 3. Except for the BNU-ESM model, the rest of models have a relatively poor performance. The simulated precipitation value in May and June is much larger than the measured precipitation except for the CNRM-CM5 and MRI-CGCM3 model. The maximum value of the measured precipitation occurs in July while that of the MIROC-ESM model occurs in June. In overall, the annual distribution simulation results of BNU-ESM, MME-AM, and MPI-ESM-LR model are more consistent with the measured precipitation process. The monthly precipitation and the variance trend of BNU-ESM model are similar to the measured data which has the best performance among the entire selected climate models.

Fig. 3 The annual distribution of precipitation simulated by each model during the baseline period (1960–2000)



4.2 Simulation of spatial distribution

The four seasons in the Huaihe River basin are spring (from March to May), summer (from June to August), autumn (from September to November), and winter (from December to February). Figure 4 illustrates the spatial distribution of measured data during baseline period. The annual precipitation of the Huaihe River basin decreases from south to north, and precipitation in the mountain area is larger than that in the plain area while that in the coastal area is larger than that in the inland region. The precipitation mainly occurs in the spring and summer season. Precipitation in summer in most

part of the Huaihe River basin ranges between 400 and 500 mm, while that in the coastal areas and the south mountain area are larger than 500 mm.

We interpolate the global climate data of each year during the baseline period into the whole basin by using the Inverse Distance Weighted (IDW) method. Figure 5 draws the spatial distribution map of relative error between the simulated result of BNU-ESM model and the measured data. As can be seen from Fig. 5, the simulation performance of BNU-ESM model in spring and winter is less effective and the simulation value is higher than the measured data in most places, and the place where the

Fig. 4 Spatial distribution of measured precipitation data in different time scales: (a) spring, (b) summer, (c) autumn, (d) winter, and (e) annual during the baseline period

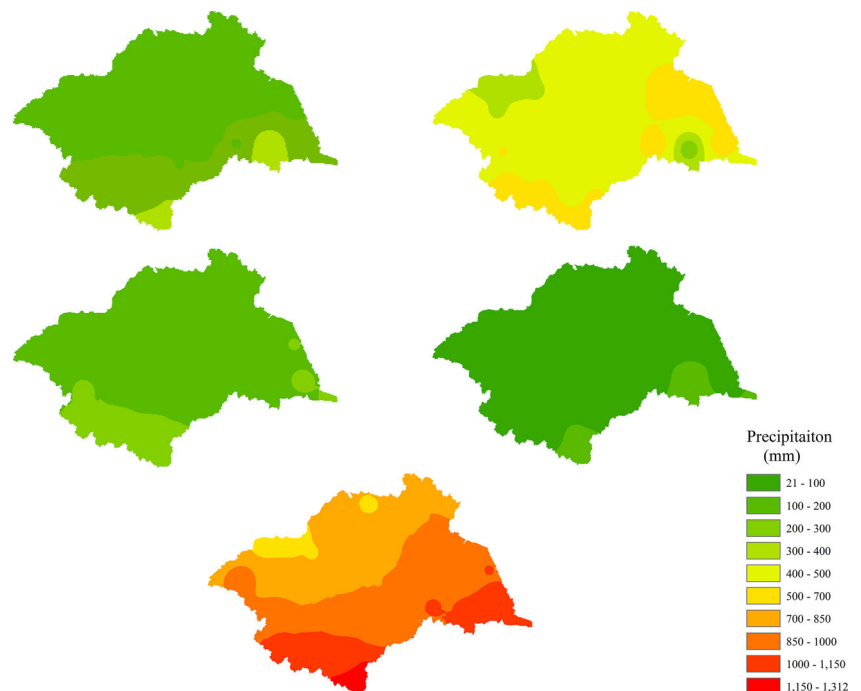
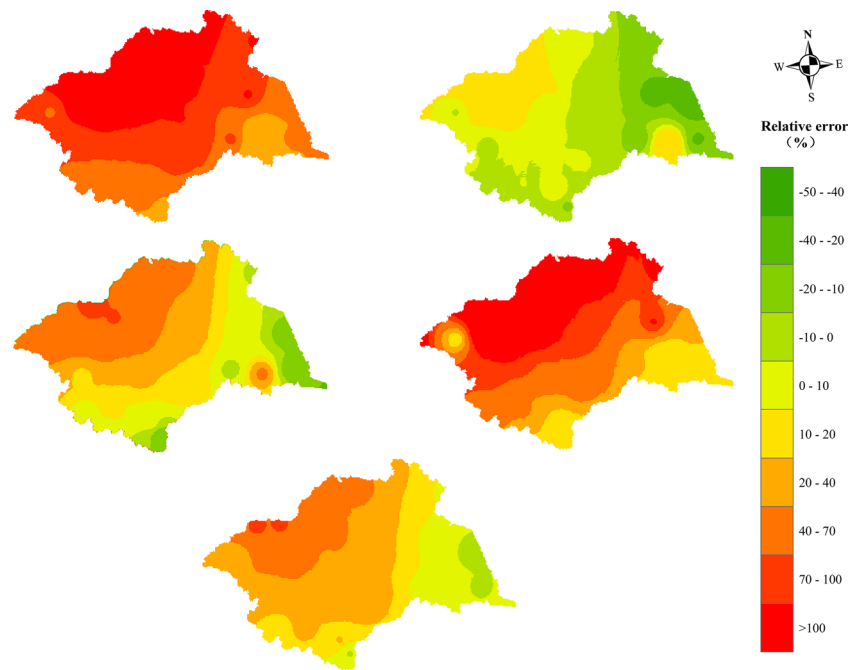


Fig. 5 The spatial distribution of relative error in different time scales: (a) spring, (b) summer, (c) autumn, (d) winter, and (e) annual precipitation simulated by BNU-ESM model compared with the measured data during the baseline period



relative error is more than 100% accounting for 30% of the area of the Huaihe River basin. The simulated summer precipitation in the central and southern area has a good simulation performance where the relative error ranges between $\pm 10\%$, and the coastal and the northwest of the area have a larger relative error. As can be seen from the relative error distribution map of autumn season, the simulated value is larger than the measured data in most areas, moreover, the area where the relative error is greater than 20% accounting for 51.5% of the basin. The spatial distribution of annual precipitation simulated by BNU-ESM model is higher than the measured value in most area, and the places where the relative error is greater than 20% accounting for 62% of the basin area. The coastal area of Jiangsu provinces has the good simulation results where relative error is less than 10%. Overall, the simulation result of BNU-ESM model is higher than the measured value in each season while the simulation performance are poor in the northwest of the basin, and the difference between the simulated and the measured data decreases from the northwest to the southeast.

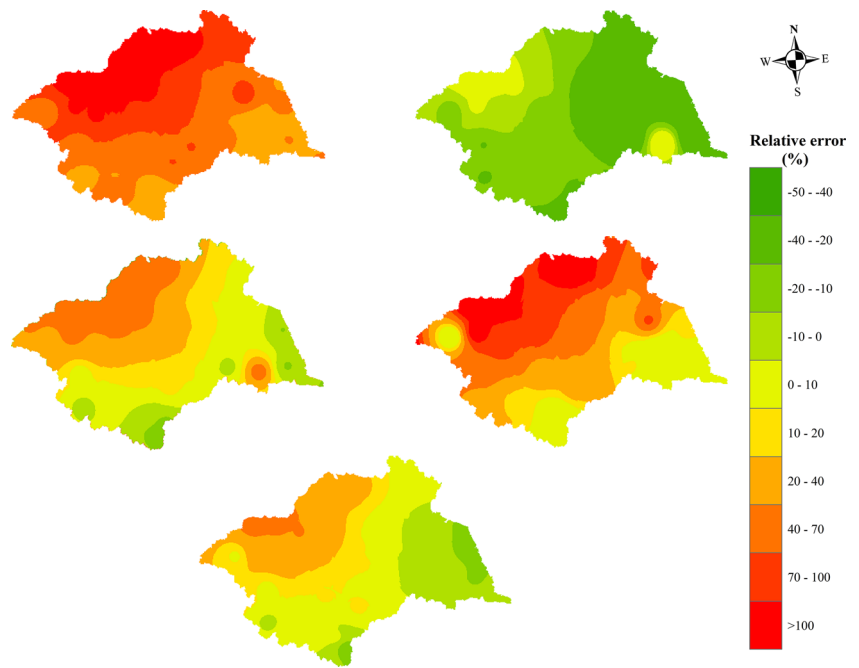
Figure 6 is the spatial distribution map of relative error between the MME-AM simulated output and the measured data. The MME-AM model has a poor simulation in spring and winter, and the simulation results are larger than the measured data in most areas. Although the relative error in the northern part of the basin is still larger than 100%, the simulation results are better than the BNU-ESM model. As can be seen from the spatial distribution map of the relative error in summer, the relative error in most areas ranges between $-10\sim-40\%$ and the simulation effects are worse than the

BNU-ESM model. The precipitation simulation results are higher than the measured data in autumn, the relative error in the northwest area is much higher and it ranges between 20 and 70%. The simulated annual precipitation of MME-AM model during baseline period shows a decreasing trend from northwest to southeast, the relative error which is accounting for 54% of the basin area ranges between $\pm 10\%$. Overall, the MME-AM model homogenizes the result, that is, the simulation results in low-precipitation season are higher than the measured data while in the high-precipitation season are lower than the measured data. In general, the simulation performance of MME-AM model is better than the BNU-ESM model.

4.3 Spatial calibration

Taking the annual precipitation spatial distribution as an example, we calibrate the simulation results of BNU-ESM model and MME-AM model during validation period using the Delta method and compare the calibrated results to the measured data. Figure 7 shows the spatial distribution of relative error of calibrated BNU-ESM model and calibrated MME-AM model compared with the measured data, the relative error obviously decreases after spatial calibration. The relative error of calibrated BNU-ESM model which ranges from -5 to 30% is taking up 70% of area of total area. The calibrated simulation result of MME-AM model is smaller than the measured data, and the relative error ranges between -10% and 0 . The area where relative error ranges between $-5\sim-7.5\%$ accounts for 65% of the total area.

Fig. 6 The spatial distribution of relative error in different time scales: (a) spring, (b) summer, (c) autumn, (d) winter, and (e) annual precipitation simulated by MME-AM model compared with the measured data during the baseline period



5 Simulation of precipitation by BP neural network during baseline period

5.1 Simulation result of the average rainfall process in the basin

We take the annual precipitation data from the year of 1960 to 2000 of each climate model as the input data and fit with the measured annual precipitation series. The training time of the model internal parameters is about 20,000 times. Figure 8

shows the result of MME simulated by the BP neural network during training period and validation period. The simulation effect is much better than the MME-AM model, the deterministic coefficient is 0.819 during the baseline period and 0.814 during the validation period.

5.2 Spatial distribution result of simulated precipitation

Figure 9 is the spatial distribution map of relative error of MME-BP model during the validation period compared

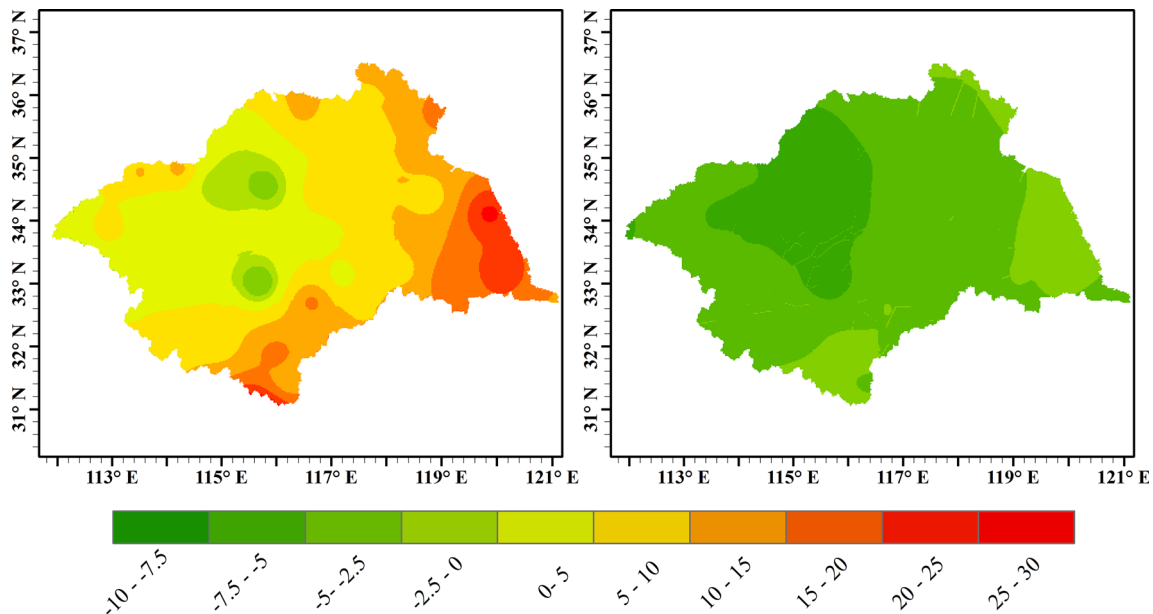
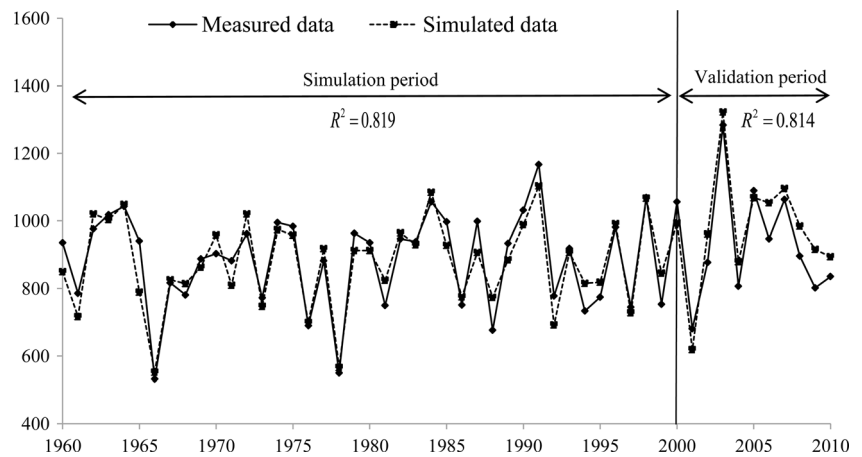


Fig. 7 The relative error spatial distribution of annual precipitation simulated the (a) calibrated BNU-ESM model and (b) calibrated MME-AM when comparing to the measured data during the validation period

Fig. 8 Comparisons between the measured data and MME-BP output during the training period and validation period



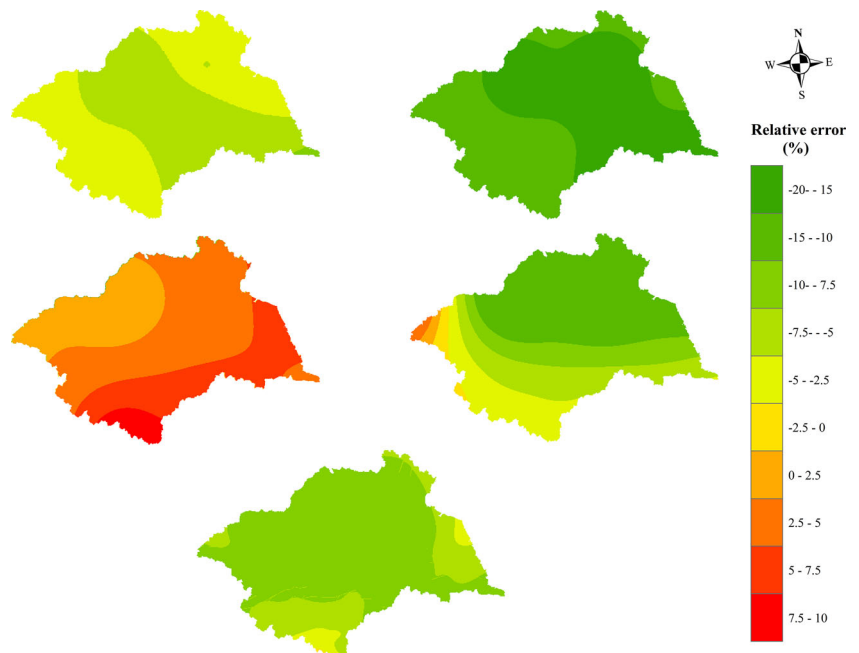
with the measured data. The simulation performance during spring season is good while the simulation result of the whole basin is smaller than the measured data and the relative error ranges between $-2.5\sim-7.5\%$. During the summer season, the simulated value is less than the measured data. The places where the relative error ranges between -15 and -20% account for 54% of the total area. The relative error in the rest places ranges between -10 and -15% . The simulated precipitation value in autumn is higher than the measured value, and the relative error increases from north to south and ranges from 0 to 10% . The simulated precipitation of the most areas in winter is lower than the measured data, the places where the relative error is higher than -10% accounting for 47% of the total area. As can be seen from the simulation effect of

annual precipitation, the simulated value is lower than the measured data. The places where the relative error ranges between -7.5 and -10% account for 76% of the whole basin. As can be seen from the spatial distribution map of annual precipitation, the simulation performance of MME-BP model is similar to calibrated MME-AM model and better than the calibrated BNU-ESM model.

6 Future climate prediction

In this paper, possible climate changes in the future are analyzed by the six kinds of calibrated climate models, the calibrated MME-AM model and the MME-BP model. We emphatically analyze the prediction result of high performance

Fig. 9 The spatial distribution of relative error in different time scales: (a) spring, (b) summer, (c) autumn, (d) winter, and (e) annual precipitation simulated by MME-BP model compared with the measured data during the validation period



model named calibrated BNU-ESM, calibrated MME-AM, and MME-BP. The prediction period is from the year of 2011 to 2100.

6.1 Linear trend and annual distribution of precipitation in future climate change

Table 2 shows the predication results of the linear trend of annual precipitation in the Huaihe River basin during 2011–2100. The annual average precipitation of all models shows an increasing trend and the magnitude of variation is significantly different from 12.3 to 107.5 mm/100a. The magnitude of variation of calibrated BCC-CSM-1.1 model and MME-BP model are relatively small which are about 12.3 and 20.2 mm/100a, respectively. The calibrated MPI-ESM-LR has the largest variation with 107.5 mm/100a. The variation of calibrated BNU-ESM model is close to the average variation which is 67.9 mm/100a.

Figure 10 shows the change between annual distributions of predicted precipitation by each calibrated model during future three time periods and the monthly precipitation during baseline period. During the time decade of 2020s, the precipitation shows a decreasing trend in the month of July, August, and October while that in the rest of months shows an increasing trend. For example, the 50% quantile of precipitation in July and August are -18.6 and -11.7%, respectively. During the time decade of 2050s, the precipitation of each month shows an increasing trend except for the month of January, June to August, and October. During the time period of 2080s, the precipitation of each month shows an increasing trend except for the month of July to September. Overall, in different future time periods, the monthly precipitation during June to October decrease or increase in a minimum range, which may reduce the pressure of flood control in the Huaihe River basin. The maximum increased periods of precipitation during different time period are different. During 2020s, the precipitation in February increased to the largest extent which is 27.9 in 50% quantial. During

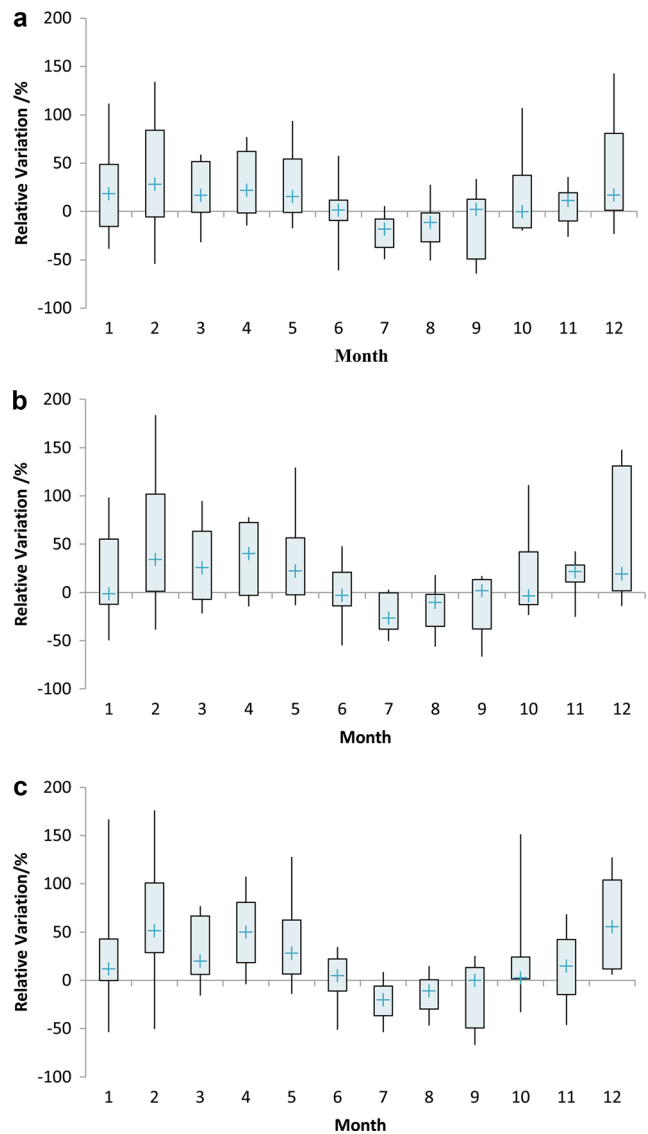


Fig. 10 The annual distribution of precipitation in the next three time periods of **a** 2020s, **b** 2050s, and **c** 2080s

2050s, the precipitation in April increased to the largest extent which is 40.2 in 50% quantial. During 2080s, the precipitation in December increased to the largest extent which is 55.7 in 50% quantial.

Table 2 The linear trend of annual precipitation in Huaihe River basin predicted by each model from Tables 2011 to 2100

Model	Precipitation variation mm/100a	Model	Precipitation variation mm/100a
BCC-CSM-1.1	12.3	MPI-ESM-LR	107.5
BNU-ESM	67.9	MRI-CGCM3	105.5
MIROC-ESM	91.1	MME-AM	72.8
CNRM-CM5	82.7	MME-BP	20.2
		Mean	70

6.2 Change of precipitation during the future climate decade

We analyze the prediction result of calibrated BNU-ESM with high simulation performance, calibrated MME-AM, and MME-BP model, and the seasonal changes between predicted precipitation in different decades and precipitation during baseline period in the Huaihe River basin during the twenty-first century are shown in Table 3. The annual precipitation of calibrated BNU-ESM model, calibrated MME-AM, and MME-BP model all shows an increasing trend during the

Table 3 Precipitation change rate simulated by three models at different time scales during the future time periods

Model	Time period	Precipitation variation rate (%)				
		Spring	Summer	Autumn	Winter	Annual
BNU-ESM	2020s	7.70	-2.59	14.50	13.87	4.17
	2050s	10.32	-1.09	6.19	-0.41	2.86
	2080s	16.86	6.23	-1.73	25.59	8.31
MME-AM	2020s	2.44	3.96	2.93	5.00	3.50
	2050s	8.33	2.67	6.62	12.99	5.40
	2080s	13.99	5.30	5.52	22.56	8.43
MME-BP	2020s	2.69	1.54	0.27	21.97	5.26
	2050s	1.34	2.77	-10.28	20.40	3.98
	2080s	13.99	-1.31	-10.39	9.53	2.12

decades of 2020s, 2050s, and 2080s. The variation rate of annual precipitation predicted by calibrated BUN-ESM model during future periods ranges from 2.86 to 8.31%. Precipitation variation rate of calibrated BNU-ESM during spring has large magnitude which ranges from 7.7~16.86%. The precipitation variation rate in summer season decreases in 2020s and 2050s while increases by 6.23% during 2080s. In autumn, the variation rate increases by 6.19 and 14.5% during 2020s and 2050s, respectively, and it decreases by 1.73% during 2080s. In winter season, except for a slight decrease in 2050s, precipitation increases significantly during 2020s and 2080s.

As can be seen from Fig. 11, the future seasonal and annual precipitation predicted by calibrated MME-AM model shows an increasing trend, and the precipitation variation rate in spring and winter are relative larger than the precipitation during baseline period. The change rates of annual precipitation range from 3.5 to 8.43%. The change rates of precipitation in spring, summer, autumn, winter seasons are 2.44~13.99%, 2.67~5.3%, 2.93~6.62%, and 5~22.56%, respectively.

The precipitation predicted by MME-BP model shows an increasing trend in annual precipitation which is about 2.12~5.26%. Among the four seasons of 2020s, precipitation in winter increases obviously, which is increased about 21.97%. In 2050s, except for the autumn precipitation which will reduces about 10.8%, precipitation in the rest of all season increases. In 2080s, precipitation in summer and autumn seasons will decrease about 1.31 and 10.39% comparing to the baseline period. The precipitation in spring and winter season is increased largely which is about 13.99 and 9.53%, respectively. A comprehensive overview of the prediction results by the three models in the future climate change, the future annual precipitation shows an increasing trend. The future precipitation of some season is decreased in different time period, mainly concentrate in summer and autumn seasons.

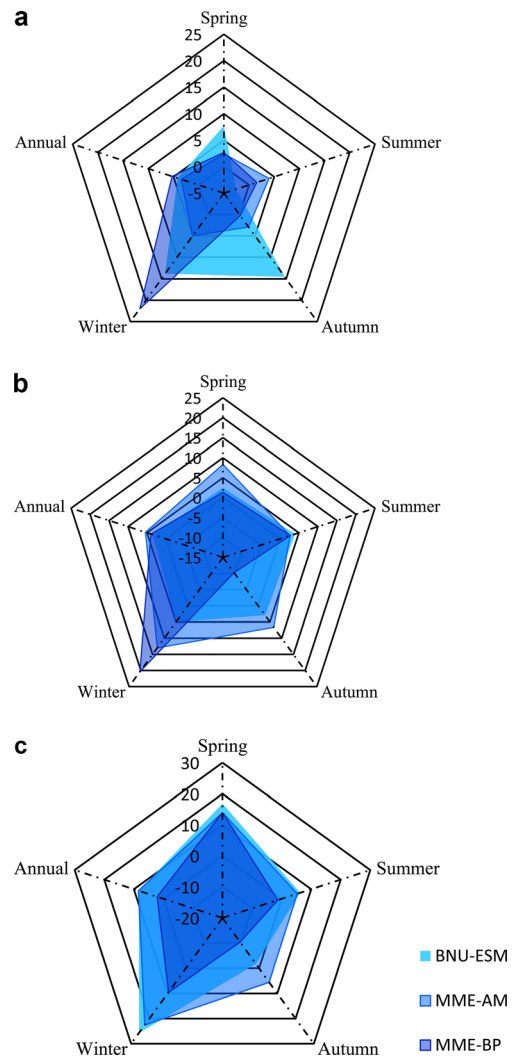


Fig. 11 Variations of precipitation predicted by different models in the future decades: **a** 2020s; **b** 2050s; **c** 2080s

6.3 Spatial distribution of future precipitation

Figure 12 illustrates the spatial distribution of precipitation variation between precipitation predicted by calibrated BNU-ESM, calibrated MME-AM, and MME-BP models and precipitation during the baseline period. It can be seen that the variation of precipitation gradually increases from northwest to the southeast, and the increased amplitude of precipitation on the right bank is larger than the left bank, while that on the downstream is larger than that on the upstream. The future precipitation in the most area of the Huaihe River basin increase during each time period except for the precipitation in 2020s predict by the MME-BP model which reduces about 10 mm. As can be seen from the results during 2020s, the predict precipitation results of the three models increase from the northwest to the southeast of the basin. The prediction variation of calibrated BNU-ESM model is relatively concentrated, the places which increased about

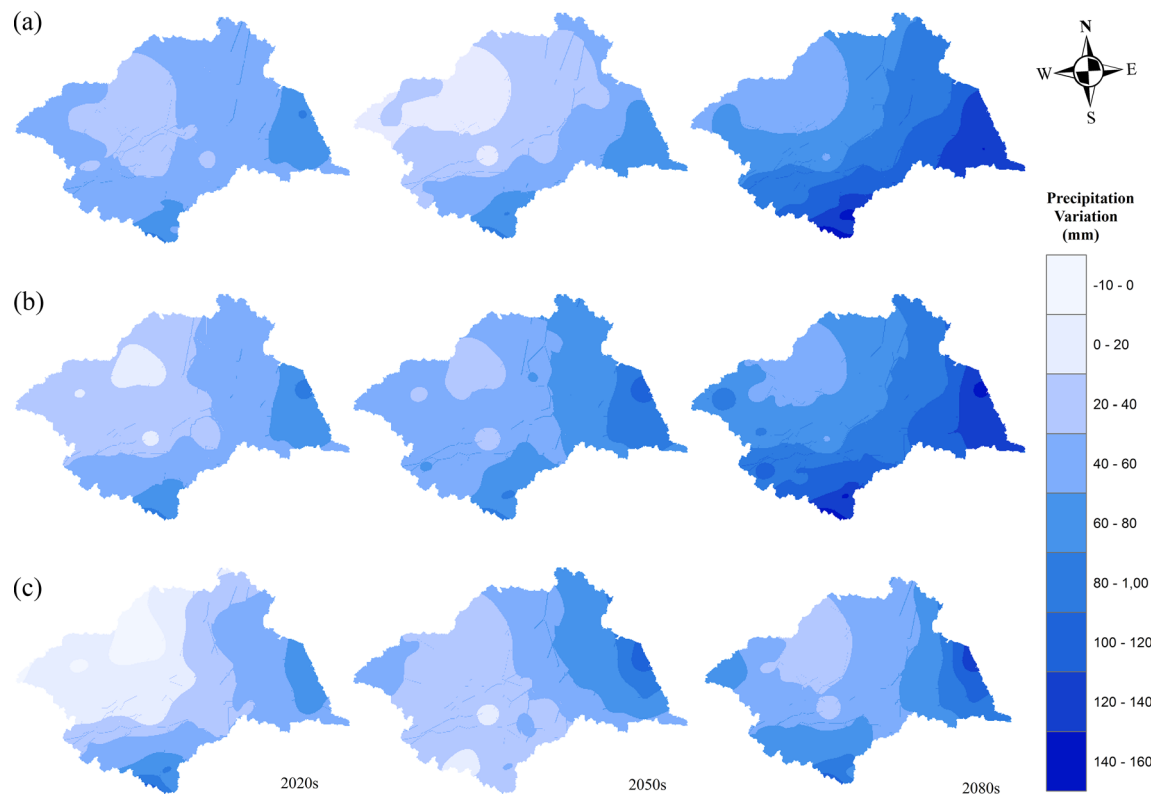


Fig. 12 The spatial variation distribution of precipitation between three models: (a) BNU-ESM; (b) MME-AM; (c) MME-BP and measured data in different time periods

40~60 mm take up 64.4% of the area of the Huaihe River basin. The precipitation in the places which are located in the northwest of the Huaihe River basin decreases about $-10-0$ mm, these regions cover 8% of the Huaihe River basin.

During the time period of 2050s, the precipitation predicted by calibrated MME-AM has the largest increase amplitude ranges from 20~120 mm, these places cover 50.6% of the area of the Huaihe River basin changes between 40 and 60 mm. the precipitation variation results predicted by calibrated BNU-ESM and MME-BP are mainly concentrated in 20–40 mm,

accounting for 42.9 and 47.2% of the whole basin, respectively.

In 2080s, the spatial distribution of precipitation variation predicted by calibrated BNU-ESM model is similar to the calibrated MME-AM which mainly concentrates between 60 and 100 mm and these regions cover 53 and 61% of the area of the Huaihe River basin. The spatial distribution of precipitation variation predicted by MME-BP model mainly concentrates between 40 and 80 mm, accounting for 70.9% of the Huaihe River basin (Table 4).

Table 4 The area of precipitation variation predicted by three models during future decades

Time period	Model name	Precipitation variation (mm)								
		-10	0–20	20–40	40–60	60–80	80–100	100–120	120–140	140–160
2020s	BNU-ESM			23.2	64.4	12.1	0.3			
	MME-AM		5.4	41.1	40.9	11.7	0.9			
	MME-BP	8	31.1	23.2	28.5	8.2	0.8	0.1		
2050s	BNU-ESM		18.9	42.9	25.6	12.3	0.3			
	MME-AM			8.6	50.6	30.7	9.2	1		
	MME-BP		2.6	47.2	26.4	19.3	3.4	1		
2080s	BNU-ESM				20.2	27.1	25.9	14.3	11.6	0.8
	MME-AM				13.1	33	28	15.5	9.5	0.8
	MME-BP			16.5	43.8	27.1	8.5	3.2	0.8	

7 Discussion and conclusion

In this paper, the outputs of six GCMs from CMIP5 are used to evaluate the precipitation simulation performance on Huaihe River basin. Besides, two multimodel ensembles are obtained by arithmetic mean method and BP neural network, MME-AM and MME-BP, respectively. Thereafter, the delta method is used to calibrate single climate model data and MME-AM output and rebuild the future climate series. After that, we predict the characteristics of precipitation change in the Huaihe River basin during twenty-first century by using the calibrated single climate model, calibrated MME-AM, and MME-BP model. The main conclusions are shown below:

1. The six kinds of global climate models and MME-AM have a certain simulation performance on precipitation process in the Huaihe River basin. The simulation results are quite different, and the multiyear average precipitation of four single models and MME-AM are overestimated. The MME-AM model has a higher correlation coefficient but did not show the best simulation capability. By using the Taylor diagram involving three index, standard deviation, correlation coefficient, and RMSE, the order of simulation ability on precipitation process of each model is: BNU-ESM > MME-AM > CNRM-CM5 > MRI-CGCM3 > MIROC-ESM > BCC-CSM-1.1 > MPI-ESM-LR.
2. An analysis of interannual distribution shows that three models named BNU-ESM, MME-AM, and MPI-ESM-LR model are consistent with the measured precipitation process. The BNU-ESM model has the best simulation performance, the maximum monthly precipitation of other models occurred in June which are not the same with the observed precipitation occurred in July. According to the spatial distribution of precipitation difference between the simulated value and measured value, the spatial simulation capability of MME-AM is better than the BNU-ESM model.
3. Six kinds of global climate models are used as the input of BP neural network, and we obtain the output results after training the BP neural network. The annual mean precipitation series simulated by MME-BP model has a good fitting effect. The deterministic coefficient during the baseline period and the validation period are 0.819 and 0.814, respectively. The model of MME-BP has good spatial simulation ability, the spatial distribution deviation of the simulation results in spring, autumn, and winter seasons are small. The effect of spatial simulation ability is ranked as: calibrated MME-AM > MME-BP > MME-AM > calibrated BNU-ESM > BNU-ESM.
4. The linear trend of future precipitation demonstrates that the results predict by all models are show an increasing trend. Among all the models, the calibrated BCC-CSM-1.1 model and MME-BP model increase slightly. As can

be seen from the annual distribution, the monthly precipitation during June to October decrease or increase slightly which may relieve the flood control pressure. The predicted results of future precipitation based on the model of calibrated BNU-ESM, calibrated MME-AM, and MME-BP show that precipitation during 2020s, 2050s, and 2080s tend to increase. The rank of average growth rate of the three models in each season is: winter > spring > summer > autumn. The precipitation during winter and spring increases significantly which can ease the pressure on water supply. The precipitation during summer and autumn increases slightly which means the future flood situation in Huaihe River basin is still grim.

5. The precipitation variation in the twenty-first century predicted by calibrated BNU-ESM, calibrated MME-AM, and MME-BP models are distinctive, but there is an agreement that the precipitation tend to increase in the future. The increased amplitude on the right bank of the Huaihe River basin is larger than that in the left bank and the downstream is larger than the upstream. The amplitude ranges from 0 to 160 mm and increases with the growing time period, the rank of average increase rate of the three time periods is: 2080s > 2050s > 2020s.

In this paper, we attempt to use BP neural network to fit a variety of climate models and apply the outputs results of BP neural network (MME-BP), the GCMs, and the MME-AM model to evaluate the simulation performance on precipitation. The simulation results indicate that only a few models show a better agreement with the observations. Due to the coarse resolution of the current global climate model, the estimation of future climate remain highly uncertainties. There is room for reducing the uncertainty of regional climate change prediction.

Acknowledgements This study is supported by the National Natural Science Foundation of China (Grant No. 51579068/51609062), the Special Fund for Public Welfare Industry of the Ministry of Water Resources of China (Grant No. 201501007), and the National Key Technologies R&D Program of China (Grant No. 2016YFC0400909).

References

- Chen L, Frauenfeld OW (2014) A comprehensive evaluation of precipitation simulations over China based on CMIP5 multimodel ensemble projections. *J Geophys Res-Atmos* 119:5767–5786
- Croke B, Islam A, Ghosh J, Khan M (2011) Evaluation of approaches for estimation of rainfall and the unit hydrograph. *Hydrol Res* 42:372–385. doi:10.2166/nh.2011.017
- Du Z, Huang R, Huang G (2010) A weighting ensemble method by pattern correlation coefficients in sliding windows and its application to ensemble simulation and prediction of Asian summer monsoon. *Chinese J Atmos Sci* 1168–1186 (in Chinese)

- Feng J, Lee D, Fu C et al (2011) Comparison of four ensemble methods combining regional climate simulations over Asia. *Meteorog Atmos Phys* 111:41–53
- Gao C, Jiang T, Zhai J (2012) Analysis and prediction of climate change in the Huaihe River basin. *Chin J Agrometeorol* 8–17 (in Chinese)
- Hay LE, Wilby RL, Leavesley GH (2000) A comparison of delta change and downscaled GCM scenarios for three mountainous basins in the United States. *J Am Water Resour Assoc* 36:387–397. doi:10.1111/j.1752-1688.2000.tb04276.x
- Hirabayashi Y, Mahendran R, Koirala S et al (2013) Global flood risk under climate change. *Nat Clim Chang* 3:816–821
- Ke Z, Dong W, Zhang P, Wang J, Zhao T (2009) An analysis of the difference between the multiple linear regression approach and the multimodel ensemble mean. *Adv Atmos Sci* 26:1157–1168. doi:10.1007/s00376-009-8024-8
- Kharin VV, Zwiers FW (2002) Climate predictions with multimodel ensembles. *J Clim* 15:793–799. doi:10.1175/1520-0442(2002)015<0793:cpwme>2.0.co;2
- Li M, Lv H, Ouyang F (2012a) Analysis and prediction of climate change in Huaihe River Basin based on delta method. *YANGTZE RIVER* 11–14+46 (in Chinese)
- Li X, Xu Z, Cheng H (2012b) Projection of climate change with various emission scenarios over Huaihe River Basin in the 21st Century. *Plateau Meteorol* 1622–1635 (in Chinese)
- Lim Y, Lee J, Oh H-S, Kang H-S (2015) Independent component regression for seasonal climate prediction: an efficient way to improve multimodel ensembles. *Theor Appl Climatol* 119:433–441. doi:10.1007/s00704-014-1099-x
- Liu Y, Zhang J, Wang G, Liu J, He R, Wang H, Jin J (2012) Evaluation on the influence of natural climate variability in assessing climate change impacts on water resources: II. Application in future climate. *Adv Water Sci* 156–162 (in Chinese)
- Lu G, Yang Y, Wu Z, He H, Xiao H (2014) Temporal and spatial variations of snow depth in regions of the upper reaches of Yangtze River under future climate change scenarios: a study based on CMIP5 multi-model ensemble projections. *Adv Water Sci* 484–493 (in Chinese)
- Luo J, Lu W, Ji Y, Ye D (2016) A comparison of three prediction models for predicting monthly precipitation in Liaoyuan city, China. *Water Sci Tech-W Sup* 16:845–854. doi:10.2166/ws.2016.006
- Min Y-M, Kryjov VN, Oh SM (2014) Assessment of APCC multimodel ensemble prediction in seasonal climate forecasting: retrospective (1983–2003) and real-time forecasts (2008–2013). *J Geophys Res-Atmos* 119:12132–12150. doi:10.1002/2014jd022230
- Peng PT, Kumar A, van den Dool H, Barnston AG (2002) An analysis of multimodel ensemble predictions for seasonal climate anomalies. *J Geophys Res-Atmos* 107 doi:10.1029/2002jd002712
- Samanta S, Pal DK, Lohar D, Pal B (2012) Interpolation of climate variables and temperature modeling. *Theor Appl Climatol* 107:35–45
- Sarwar R, Irwin SE, King LM, Simonovic SP (2012) Assessment of climatic vulnerability in the Upper Thames River basin: downscaling with SDSM. The University of Western Ontario Department of Civil and Environmental Engineering
- Shoab M, Shamseldin AY, Melville BW, Khan MM (2016) A comparison between wavelet based static and dynamic neural network approaches for runoff prediction. *J Hydrol* 535:211–225. doi:10.1016/j.jhydrol.2016.01.076
- Singh UK, Singh G, Singh V (2015) Simulation skill of APCC set of global climate models for Asian summer monsoon rainfall variability. *Theor Appl Climatol* 120:109–122
- Steinschneider S, Lall U (2015) A hierarchical Bayesian regional model for nonstationary precipitation extremes in Northern California conditioned on tropical moisture exports. *Water Resour Res* 51:1472–1492
- Stocker TF, Qin D, Plattner GK et al (2013) Climate change 2013: the physical science basis intergovernmental panel on climate change, working group I contribution to the IPCC fifth assessment report (AR5). Cambridge Univ Press, New York
- Sun Q, Miao C, Duan Q (2015) Projected changes in temperature and precipitation in ten river basins over China in 21st century. *Int J Climatol* 35:1125–1141. doi:10.1002/joc.4043
- Tiwari P, Kar S, Mohanty U, Dey S, Kumari S, Sinha P (2016) Seasonal prediction skill of winter temperature over North India. *Theor Appl Climatol* 124:15–29
- Wang W, Shao Q, Yang T, Yu Z, Xing W, Zhao C (2014) Multimodel ensemble projections of future climate extreme changes in the Haihe River Basin, China. *Theor Appl Climatol* 118:405–417. doi:10.1007/s00704-013-1068-9
- Waseem M, Ajmal M, Kim U, Kim T-W (2016) Development and evaluation of an extended inverse distance weighting method for streamflow estimation at an ungauged site. *Hydrol Res* 47:333–343. doi:10.2166/nh.2015.117
- Wu D, Yan D (2013) Projections of future climate change over Huaihe River basin by multimodel ensembles under SRES scenarios. *J Lake Sci* 565–575 (in Chinese)
- Wu Y, Zhong PA, Zhang Y, Xu B, Ma B, Yan K (2015) Integrated flood risk assessment and zonation method: a case study in Huaihe River basin, China. *Nat Hazards* 78:635–651. doi:10.1007/s11069-015-1737-3
- Yang H, Yang D, Hu Q, Lv H (2015) Spatial variability of the trends in climatic variables across China during 1961–2010. *Theor Appl Climatol* 120:773–783